May 28-June 1, 2017, Napoli, Italy

CHT-17-102

EFFECTS OF NEEDLE LIFT AND FUEL TYPE ON CAVITATION FORMATION AND HEAT TRANSFER INSIDE DIESEL FUEL INJECTOR NOZZLE

S. M. Javad Zeidi, George S. Dulikravich*, Sohail R. Reddy and Shadi Darvish
Department of Mechanical and Materials Eng., MAIDROC Laboratory, Florida International University,
10555 West Flagler Street, Miami, FL 33174, USA
*Corresponding author: FAX: +1 305 348 1932 Email: dulikrav@fiu.edu

ABSTRACT In the present study, the flow inside a real size Diesel fuel injector nozzle was modeled and analyzed under different boundary conditions using ANSYS-Fluent software. A validation was performed by comparing our numerical results with previous experimental data for a rectangular shape nozzle. Schnerr-Sauer cavitation model, which was selected for this study, was also validated. Two-equation $k - \varepsilon$ turbulence model was selected since it had good agreement with experimental data. To reduce the computing time, due to symmetry of this nozzle, only one-sixth of this nozzle was modeled. Our present six-hole Diesel injector nozzle was modeled with different needle lifts including 30 μm , 100 μm and 250 μm . Effects of different needle lifts on mass flow rate, discharge coefficient and length of cavitation were evaluated comprehensively. Three different fuels including one Diesel fuel and two bio-Diesel fuels were also included in these numerical simulations. Behavior of these fuels was investigated for different needle lifts and pressure differences. For comparing the results; discharge coefficient, mass flow rate and length of cavitation region were compared under different boundary conditions and for numerous fuel types. The extreme temperature spike at the center of an imploding cavitation bubble was also analyzed as a function of time and initial bubble size

INTRODUCTION

Combustion of gasoline and Diesel fuel can emit precarious exhausts which can be hazardous for environment and can increase the level of air pollution. Since liquid fuel atomization occurs in the outlet area of the injection nozzle's orifice, controlling the mentioned phenomena can lead to a better combustion process. Cavitation of the flowing liquid fuel inside the injection nozzle occurs mainly due to sudden geometrical changes. When local pressure becomes lower than the value which is called critical pressure, that is equal to vaporization pressure in many cases, cavitation can occur. In other words, there are very small size bubbles inside the flowing liquid fuel which are not noticeable when pressure is locally high. As pressure decreases below the critical level, the radii of these bubbles increase noticeably leading to formation of voids inside liquid phase. Cavitation inside Diesel fuel injector enhances primary jet breakup inside the nozzle which is very helpful for promoting atomization and more complete combustion process [1, 2].

Bergwerk [3] simulated flow inside an orifice which was similar to a real size injector nozzle by considering effects of cavitation number, sharpness of orifice inlet and ratio of orifice length to its diameter. Bode *et al.* [4]. investigated flow inside a real size transparent nozzle. Although pressure difference in their investigation was lower than the real condition, they could observe cavitation at

the inlet of nozzle's orifice. Also, increasing pressure was introduced as a major reason for cavitation occurrence. Winklhofer *et al.* [5]. conducted one of the most important experiments which is used in many papers and theses for validation of numerical simulations. He successfully observed cavitation inception, super cavitation and choke condition inside a rectangular shape nozzle.

In recent years, two-phase cavitating flow inside direct injection fuel injectors has been a very important research area in combustion and atomization. Most of recent Diesel fuel injectors have 6-8 holes. The mentioned injector holes have approximately 150 μm in diameter, with a high speed fuel flow of the order of 600 m/s in which pressure difference between nozzle inlet and outlet increases significantly. The resultant flow in these injectors are intensely turbulent and in many cases compressible as well [6–10].

Schnerr et al. [11] by acquisition of bubble growth hypothesis could successfully arrange governing equations for simulating cavitation inside Diesel injector nozzle. Singhal et al. [12] also proposed a simplified model which is the combination of Rayleigh Plesset equation and basic transfer equation. Zeidi and Mahdi successfully predicted cavitation inside Diesel injector nozzle using Singhal cavitation model [13-15]. They concluded that although Singhal cavitation model is very time consuming in numerical simulation, this model can predict choke conditions very well in comparison with Zwart Gerber Balamri and Schnerr cavitation models. Lee and Reitz [16] developed a KIVA-3V code by acquisition of homogeneous equilibrium model in which arbitrary Lagrangian-Eulerian (ALE) was used for modeling injector needle movement. They concluded that pressure difference and farfield pressure can be critical parameters for cavitation augmentation. Salvador et al. [17] used OpenFOAM software for prediction of cavitation inside Diesel injector nozzles. Their results had a very good agreement with experimental data. Mass flow rate, momentum flux and effective injection velocity were used as criteria for comparing numerical and experimental results. Som et al. [18], based on the total stress, introduced a new criterion for cavitation inception, in which cavitation pattern can be influenced noticeably. Several parameters, such as injection pressure, fuel type and needle lift position, were used. They concluded that changing needle lift position showed that as needle lift inside Diesel injector nozzle increased, cavitation length increased too. Jia et al. [19] modelled a conical-spray injector with ANSYS-Fluent software in which they concluded that cavitation can not only effect fluid speed, but spray angle can also be influenced due to cavitation. He et al. [20] investigated influence of the needle movement on flow characteristic parameters and cavitating flow; needle movement was defined as a very critical parameter for the occurrence of cavitation. They also mentioned that increasing temperature of Diesel fuel and bio- Diesel fuel has the same effect on cavitation pattern. Sun et al. [21], by modeling real size nozzle flow using ANSYS-Fluent concluded that as cavitation starts, mass flow rate and flow coefficient decrease. They also concluded that as cavitation number increases, the mass flow rate and the flow coefficient increased at first, but then decreased. Finally, Zeidi and Mahdi [22], by developing an Eulerian Lagrangian code, were able to successfully predict cavitation inside Diesel injector nozzle. They evaluated cavitation phenomena by tracking a bubble inside a nozzle's flow. They concluded that by occurrence of cavitation, parameters such as critical pressure, bubble wall radial speed and bubble position in y direction change abruptly.

MATHEMATICAL MODEL

According to the pertinent literature [23, 24], cavitation simulation mainly was conducted by the use of three methods: homogeneous equilibrium models, multi-phase flow models, and interface tracking models. In this study, multi-phase flow model was chosen since it can account for sharp density variation in actual process of phase transformation. Therefore, based on the experience reported in similar research [17, 25, 26], Schnerr-Sauer cavitation model was used in the present investigation. In Schnerr-Sauer model, the mass conservation equation for vapor can be written as

$$\frac{\partial(\alpha\rho_{v})}{\partial t} + \nabla \cdot (\alpha\rho_{v}\vec{V}_{v}) = \frac{\rho_{v}\rho_{\ell}}{\rho} \frac{D\alpha}{Dt}$$

$$\tag{1}$$

Here, α is volume fraction of vapor, ρ_v is density of vapor, ρ_l is density of liquid, ρ is density of mixture, \vec{V}_V is velocity of vapor phase, and t is time. Mass transfer source/sink per unit volume is

$$R = \frac{\rho_{\nu}\rho_{\ell}}{\rho} \frac{D\alpha}{Dt} \tag{2}$$

Notice that number of bubbles per unit volume (n_b) can be correlated with volume fraction of vapor.

$$\alpha = \frac{n_b \frac{4}{3} \pi R_b^3}{1 + n_b \frac{4}{3} \pi R_b^3} \tag{3}$$

Hence, bubble radius (R_b) and mass transfer (R) can be calculated as functions of the volume fraction.

$$R_b = \left(\frac{\alpha}{1 - \alpha} \frac{3}{4\pi} \frac{1}{n_b}\right)^{\frac{1}{3}} \tag{4}$$

$$R = \frac{\rho_{\nu} \rho_{\ell}}{\rho} \alpha (1 - \alpha) \frac{3}{R_b} \sqrt{\frac{2}{3} \left| \frac{p_{\nu} - p}{\rho_{\ell}} \right|}$$
 (5)

Here, p_v is the local static pressure of vapor, and p is static pressure in the far field. Two important dimensionless parameters will be now defined for clarifying cavitation phenomena. Discharge coefficient, which is ratio of realistic mass flow rate to ideal mass flow rate, can be defined as

$$C_d = \frac{\dot{m}}{A\sqrt{2\rho_\ell(p_{in} - p_{back})}}\tag{6}$$

Here, \dot{m} is real mass flow rate and A is area in the section of nozzle's orifice, p_{in} is inlet pressure of the nozzle and p_{back} is outlet pressure of the nozzle. Cavitation number inside nozzle is defined by Eq. 7 in which p_v is vaporization pressure of the flow inside the nozzle.

$$K = \frac{p_{in} - p_{v}}{p_{in} - p_{back}} \tag{7}$$

Cavitation Model Validation For validating our current numerical scheme, experimental results which were obtained by Winklhofer *et al.* [5] were used. A more comprehensive investigation considering grid independency can also be found in our previous publications [13-15] in which three different grids where selected in the orifice geometry and afterwards. Velocity profile was compared with experimental data and the grid producing the results having minimal difference with experimental data was selected [15-17]. Figure 1 shows Winklhofer rectangular shape nozzle in which all of the necessary dimensions are given. Pressure was used as inlet and outlet boundary

conditions, where inlet pressure was fixed to $10 \, MPa$, while outlet pressure varied between $2 \, MPa$ to $5 \, MPa$. According to Fig. 1, inlet radius of nozzle's orifice is $20 \, \mu m$, orifice length is $1 \, mm$, inlet width of nozzle's orifice is $301 \, \mu m$ and outlet length of nozzle's orifice is $284 \, \mu m$. Figure 2 also shows computational grid in the mid plane of the Winklhofer rectangular shape nozzle. Table 1 shows initial boundary condition and turbulent model parameters which were used for simulating Winklhofer nozzle. Since Winklhofer *et al.* [5] used Diesel fuel in experimental analysis, this fuel was used in our numerical analyses. Schnerr-Sauer cavitation model was chosen in this study. Formulas that were used for number of bubble density and critical pressure are also mentioned clearly. Cavitation starts to appear when local pressure becomes lower than the critical pressure. By adding wall shear stress to vaporization pressure, critical pressure can be calculated [27].

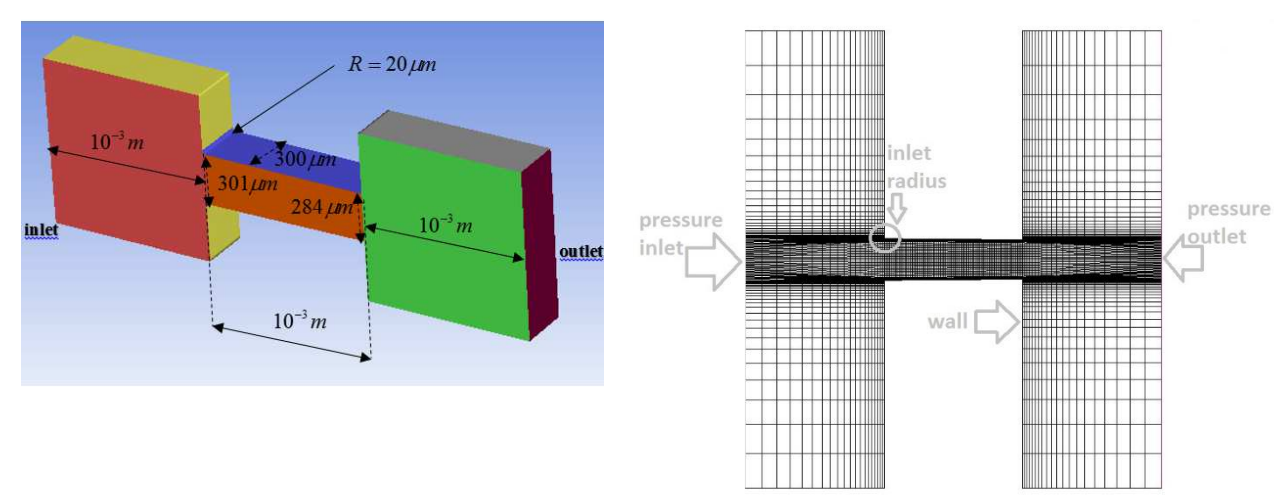


Figure 1. Winklhofer rectangular shape nozzle

Figure 2. Computational grid created for Winklhofer rectangular shape nozzle

Table 1
Input parameters and initial boundary conditions for numerical simulation

Input parameters and initial boundary conditions for numerical simulation				
		Diesel fuel (liquid)	Diesel fuel (vapor)	
	density (kg m ⁻³)	840	2.9×10^{-2}	
Physical properties	viscosity (kg m ⁻¹ s ⁻¹)	2.5×10^{-3}	3.1×10^{-6}	
	surface tension (N m ⁻¹)	2×10^{-2}	1	
	vaporization pressure (Pa)	870	-	
	Pressure inlet		10 MPa	
Initial boundary	Pressure outlet		2-5 MPa	
conditions	Turbulence intensity		$0.16 \times Re^{-1/8}$	
	Turbulence length scale		0.07D	
	Cavitation model	Schnerr-Sa	Schnerr-Sauer model	
Cavitation parameters	Number of bubbles per unit volume (m ⁻³)	$n_b = n_{ref} \times \left((p_v - p)/p_v \right)^{3/2}$		
	Critical pressure in cavitation (Pa)	$p_{cr} = p_v + 2\mu(1 + C_t \mu_t/\mu) \times S_{max}$		

According to Table 1, n_{ref} is initial estimation for number of bubble nuclei which is on the order of 1×10^{16} , S_{max} is maximum shear stress at nozzle wall which can significantly affect critical pressure, and p_{cr} is critical pressure bellow which cavitation occurs. Figure 3 shows distribution of

vapor volume fraction (α) inside Winklhofer rectangular shape nozzle. In this nozzle, cavitation inception occurs when inlet pressure is 10~MPa and outlet pressure is 4~MPa. This figure indicates that current numerical approach is able to predict cavitation inception and has a good agreement with experimental image which was obtained by Winklhofer. Figure 3 also shows occurrence of super cavitation for both experimental and current numerical approach. According to Fig. 3, our present simulation was able to predict super-cavitation and has a good agreement with the current simulation. In this type of nozzle, super cavitation occurs when inlet pressure is 10~MPa and outlet pressure is 2.5~MPa. When super cavitation occurs, vapor volume fraction extends to the outlet of orifice.

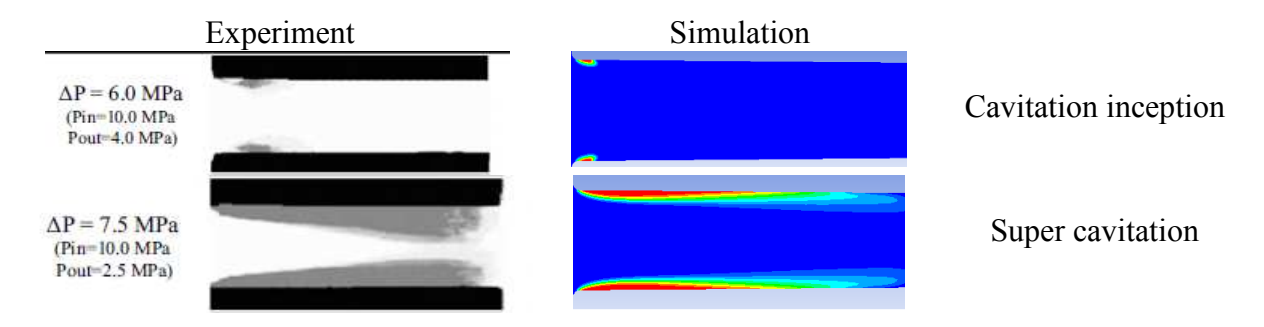


Figure 3. Distribution of vapor volume fraction inside Winklhofer rectangular shape nozzle.

Figure 4 shows velocity profile 53 μm from the orifice inlet. In the case that inlet pressure is 100 bar (10 MPa) and outlet pressure is 45 bar ($\Delta p = 55 \ bar$), no cavitation occurs. In this case, simulation with $k - \varepsilon$ turbulence model shows a better agreement with experimental data in comparison with $k - \omega$ turbulence model which shows overestimation comparing with experimental data. When $\Delta p = 67 \ bar$ cavitation occurs. In this case, simulation with $k - \varepsilon$ turbulence model has a better agreement with experimental data in comparison with simulation using $k - \omega$ turbulence model. Therefore, the rest of simulations presented here were performed with $k - \varepsilon$ turbulent model.

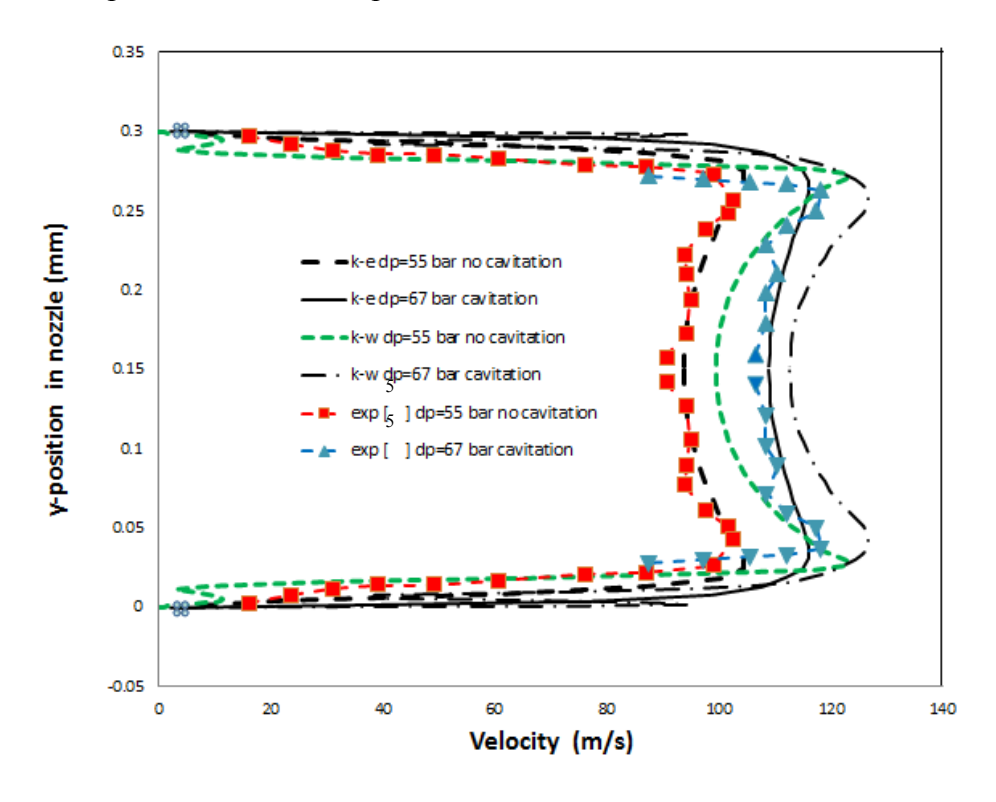


Figure 4. Predicted and measured velocity profiles at a location 53 μ m from the orifice inlet. Simulations were performed at injection pressure of 100 bar (10 MPa) and different back pressures.

NUMERICAL RESULT AND DISCUSSION

Calculation Setup and Nozzle Geometry After choosing an appropriate cavitation model and suitable turbulent model, a six-hole Diesel injector nozzle is simulated. In this real size Diesel injector nozzle, effects of needle lift and different fuel types are also investigated. In this part six-hole injector nozzle was simulated under several conditions and numerous effects such as different pressure outlets and needle lift positions were considered. In the present study, mainly effects of Diesel fuels and bio-Diesel fuels were investigated on several aspects of cavitation phenomena. In the present investigation, only one-sixth of the actual injector was modeled due to its geometric symmetry, thus, reducing calculation times significantly.

Figure 5a shows boundary conditions which were used in the current study. Figure 5b shows dimensions of the nozzle; in which, h_{max} is maximum needle lift, L is length of our nozzle's orifice, D is diameter of nozzle's orifice and r is inlet radius of nozzle's orifice. In this study, the only dimension that changes during our simulation is needle lift, h, which takes the values of $30\mu m$, $100\mu m$ and $250\mu m$ for investigating the effects of several needle lifts on occurrence cavitation.

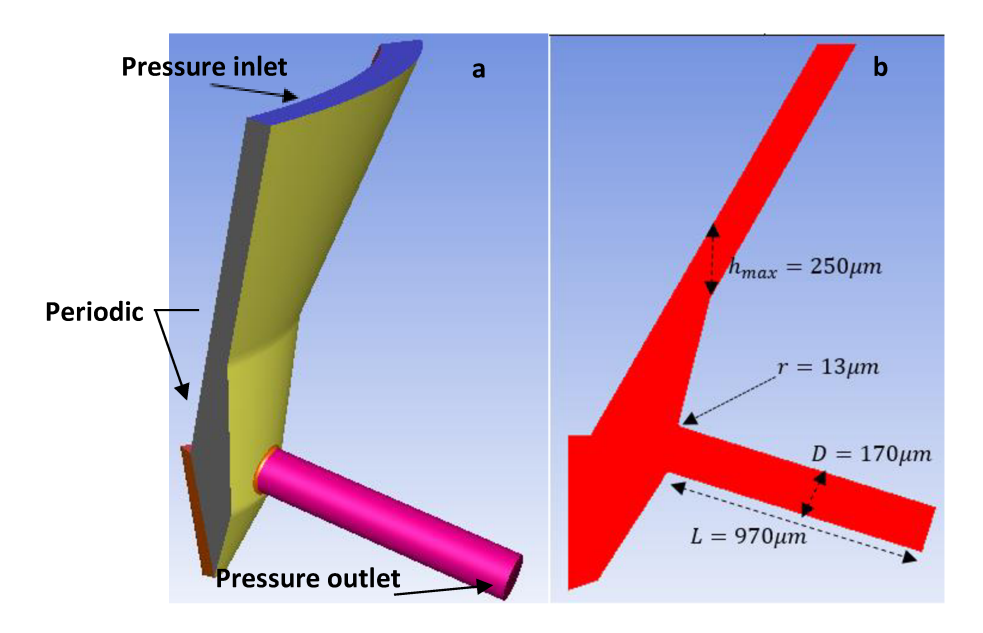


Figure 5. One-sixth of Diesel fuel injection nozzle: a) boundary conditions, and b) dimensions of the Diesel fuel injection nozzle

Table 2
Properties of three different fuels used in simulation of flow in a six-hole real size nozzle

	Diesel fuel	RME fuel	R-PVO fuel
Density (kg m ⁻³)	830	880	890
Dynamic viscosity (kg s ⁻¹ m ⁻¹)	3.61×10^{-3}	4.61×10^{-3}	6.31×10^{-3}
Vaporization pressure (<i>Pa</i>)	890	923	996
Temperature (K)	293	293	293
Number of bubbles per unit volume	1.9×10^{11}	1.9×10^{11}	1.9×10^{11}

Three types of fuels were used including two bio-Diesel fuels and a Diesel fuel which are described in Table 2, where RME1 fuels is the rapeseed methyl ester and R-PVO fuel is the rapeseed pure vegetable oil. SIMPLE numerical algorithm and two-equation $k - \varepsilon$ turbulence model with standard wall were used in the present study.

Flow boundary conditions were alike when analyzing cavitation in the Winklhofer nozzle, but inlet pressure and outlet pressures were different for the Winklhofer nozzle. In the present study, inlet pressure for the real size nozzle was fixed at 30 MPa, while outlet pressure was changed from 0.1 MPa to 9 MPa.

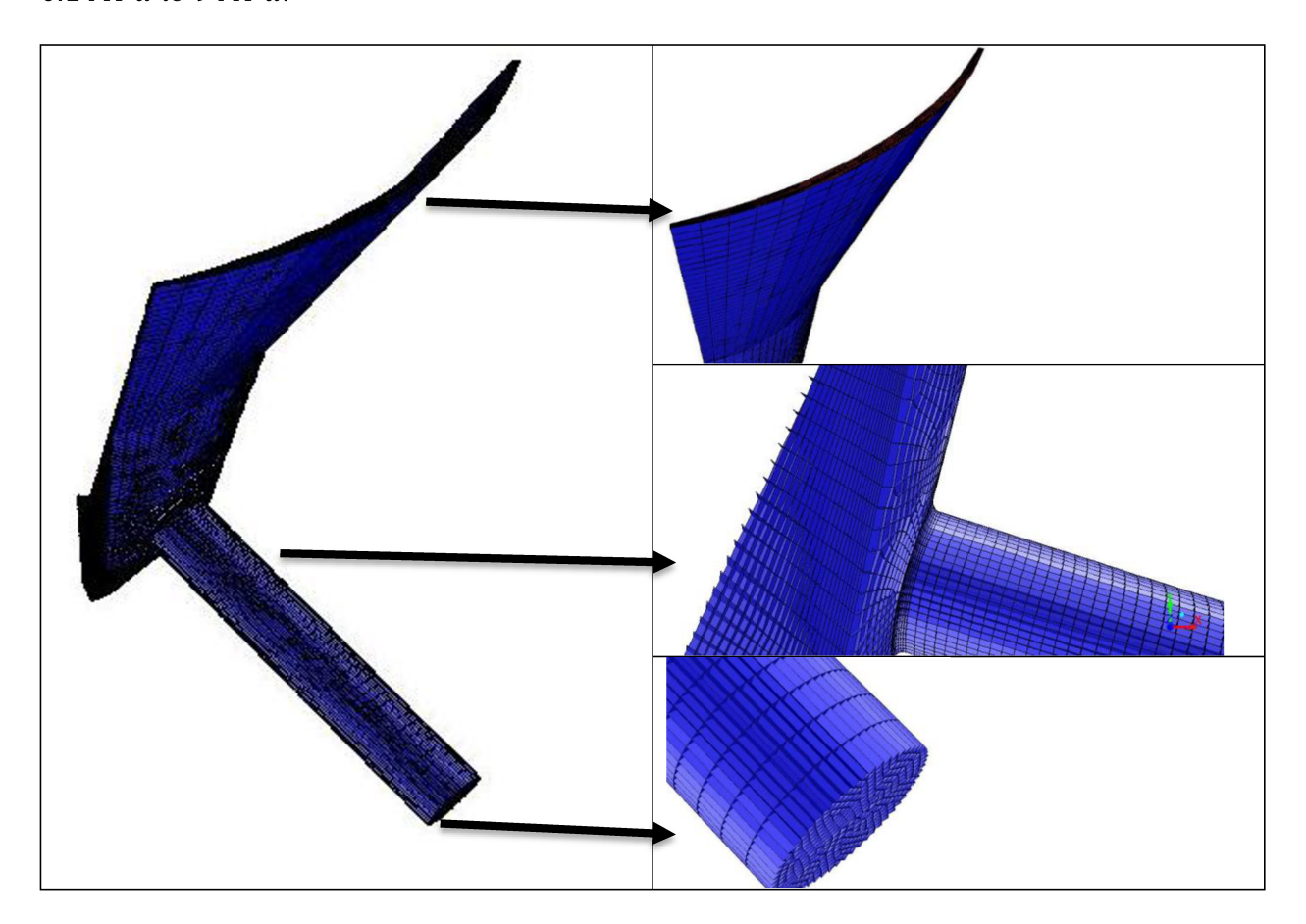


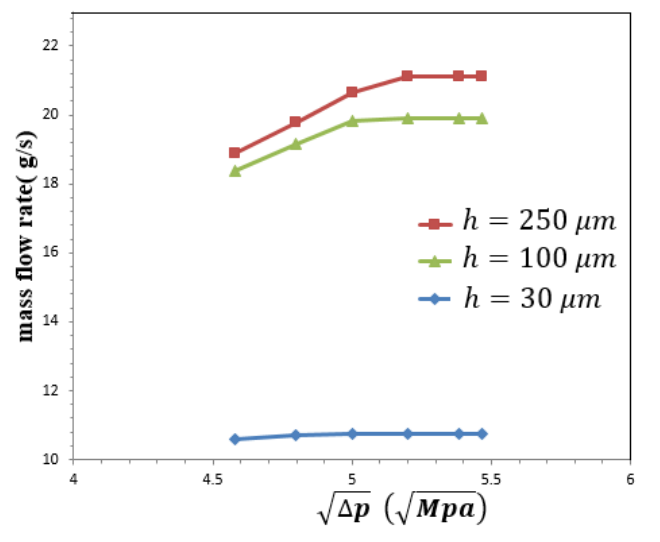
Figure 6. Computational grid for one-sixth of the injector nozzle with three different close up views

Figure 6 shows computational grid in one-sixth of the current Diesel injector nozzle. A combination of hexahedral and triangular prism grid cells was used to obtain the best results. Approximately 120000 computational grid cells were used for discretizing one-sixth of the Diesel fuel injector.

Figure 7 shows variation of Diesel fuel mass flow rate in the cases that pressure changes under three different needle lifts. In a needle lift, by increasing inlet-to-exit pressure ratio, mass flow increases, too. After a definite pressure difference (Δp), mass flow rate does not change with pressure which indicates that after this point pressure difference is not effective in controlling mass flow rate anymore. Equation 7 indicates that by increasing pressure difference, cavitation number decreases.

Figure 8 demonstrates that by decreasing cavitation number $(k^{\frac{1}{2}})$, discharge coefficient, C_d , remains stable at first, but after a while it decreases. Reason for these changes is occurrence of cavitation phenomena. Increasing pressure difference (decreasing outlet pressure), can increase cavitation length in Diesel injector nozzle. When cavitation length reaches the outlet of the nozzle's orifice, further decrease in outlet pressure will not change mass flow rate. By decreasing needle lift, mass flow rate decreases. Figure 9 shows that in the case that needle lift, h, is 100 μm or 250 μm , cavitation length does not change significantly. In other words, trends of cavitation in these two cases are similar. However, when $h = 30 \ \mu m$, mass flow rate and discharge coefficient decrease intensely

and location of cavitation occurrence changes (Fig. 9c). According to Fig 10c, when needle lift is small, cavitation occurs near the injector's needle.



0.8
0.75
0.7
0.65
0.6 $h = 250 \mu m$ $h = 100 \mu m$ $h = 30 \mu m$ 0.5
0.45
0.4
0.35
0.3
1.105
1.11
1.15
1.2

Figure 7. Variation of mass flow rate for different pressure ratios across the injection nozzle for Diesel fuel

Figure 8. Variation of discharge coefficient for different cavitation numbers for Diesel fuel

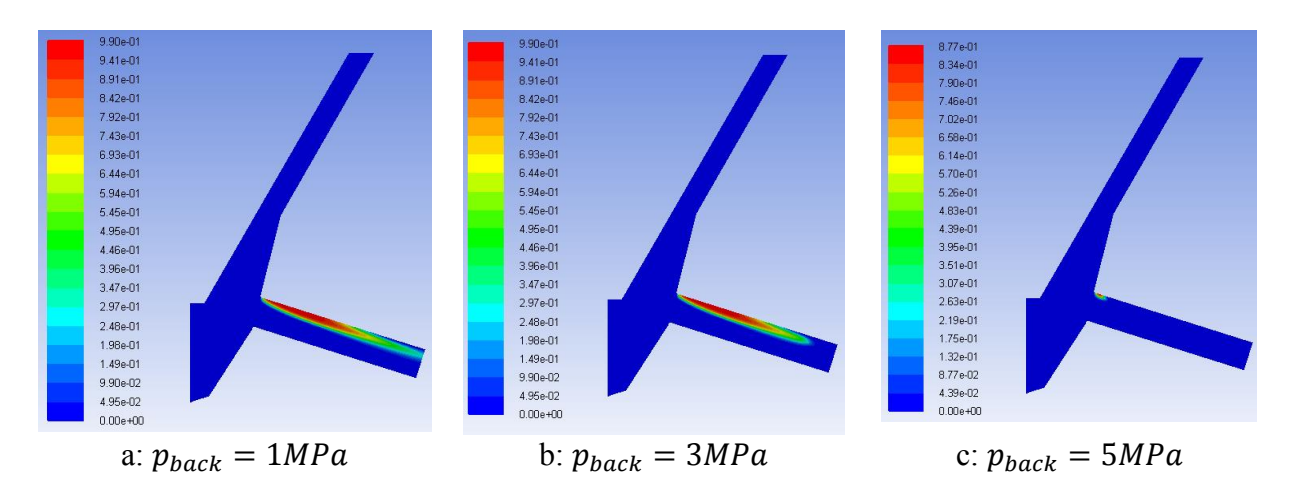


Figure 9. Distribution of vapor volume fraction in mid-plane of the nozzle for Diesel fuel in three different back pressures ($p_{in} = 30MPa$, $h = 250 \mu m$)

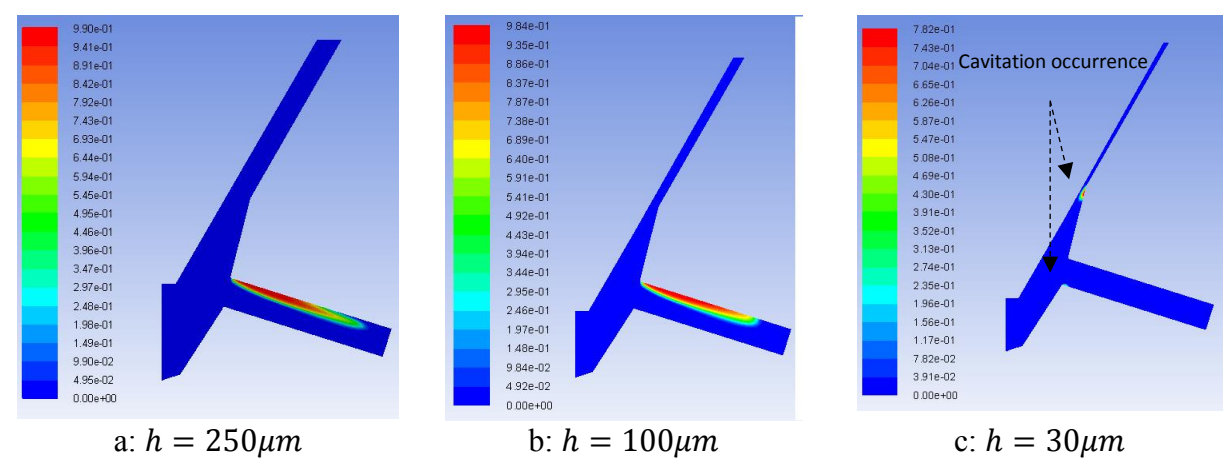
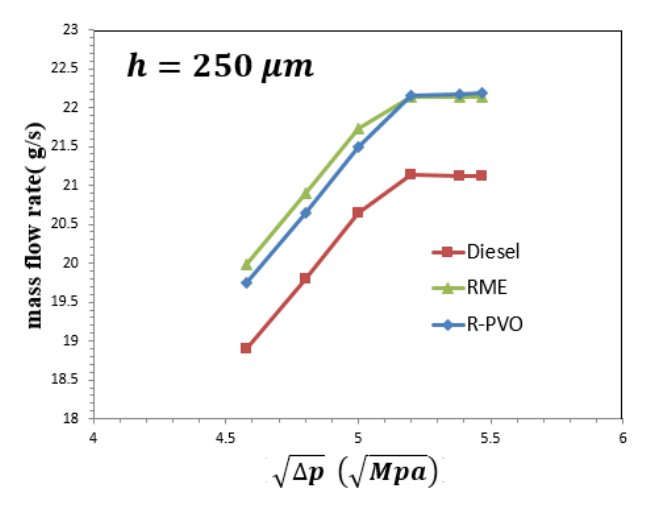


Figure 10. Distribution of vapor volume fraction in mid-plane of the nozzle for Diesel fuel in three different needle lifts ($p_{in} = 30MPa$, $p_{back} = 3MPa$)



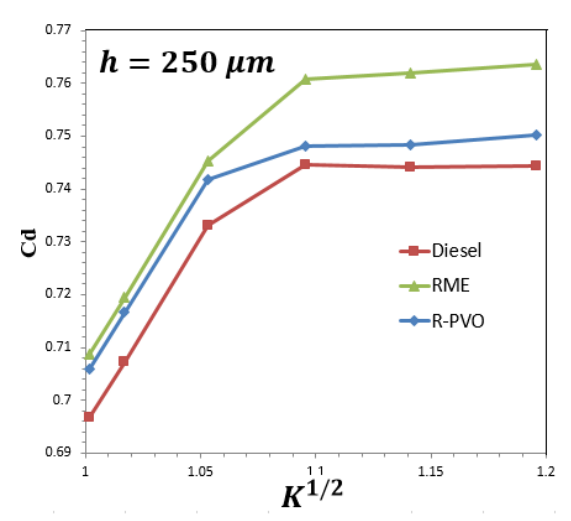


Figure 11. Variation of mass flow rate when pressure difference changes for three different fuels

Figure 12. Variation of discharge coefficient when cavitation number changes for three different fuels

Figure 11 shows that as pressure difference increases, mass flow rates increase in the case when needle lift is $250 \, \mu m$. According to this figure, mass flow rate is dependent on pressure difference, but as pressure difference increases, mass flow rate doesn't change anymore. This shows that in high pressure difference mass flow rate is not dependent on pressure difference anymore. Figure 11 also considers effects of different fuels on mass flow rate versus pressure difference. Since densities of bio-Diesel (RME and R-PVO) are higher than that of Diesel fuel, their mass flow rate is higher. Due to higher surface tension of R-PVO comparing with RME, mass flow rate of R-PVO is lower than RME when cavitation length is short. But, as cavitation length increases, effect of surface tension on mass flow rate decreases. Therefore, by increasing pressure difference, mass flow rate is not dependent on surface tension. Thus, the three fuels which are mentioned in Fig. 11 have similar trend and after a definite pressure difference, their mass flow rates do not change anymore.

Figure 12 shows variation of discharge coefficient versus cavitation number in three different fuel types. Since density of Bio-Diesel (RME and R-PVO) is higher than Diesel fuel, discharge coefficients for bio-Diesel fuels are significantly higher than for Diesel fuel. Since density of two bio-Diesel fuels are approximately equal, it is anticipated that their discharge coefficients become equal. However, for cavitation numbers higher than the critical cavitation number (K_{cr}), critical cavitation number occurs when cavitation starts, discharge coefficients of two bio-Diesel fuels do not have similar trends anymore. This difference between the trends of two bio-Diesel fuels after critical cavitation number is mainly due to differences in their surface tensions. Higher surface tension of R-PVO can lead this fuel to have higher discharge coefficient in comparison with RME, although their densities are nearly equal. In summary, after occurrence of critical cavitation number, discharge coefficient does not change by increasing cavitation number.

Figure 13 shows distribution of vapor volume fraction in mid-plane of nozzle when two types of bio-Diesel fuels and one type of Diesel fuel is used. As this figure shows, Diesel fuel has lower surface tension in comparison with two other types of fuel, so cavitation length when inlet and outlet pressures are equal for three types of fuel is noticeably higher for Diesel fuel. Furthermore, RME has greater cavitation length as Fig. 13b shows due to its lower surface tension in comparison with R-PVO bio-Diesel fuel. To sum it up, in the same boundary condition for different fuel types, those fuels that have lower surface tension have longer cavitation length.

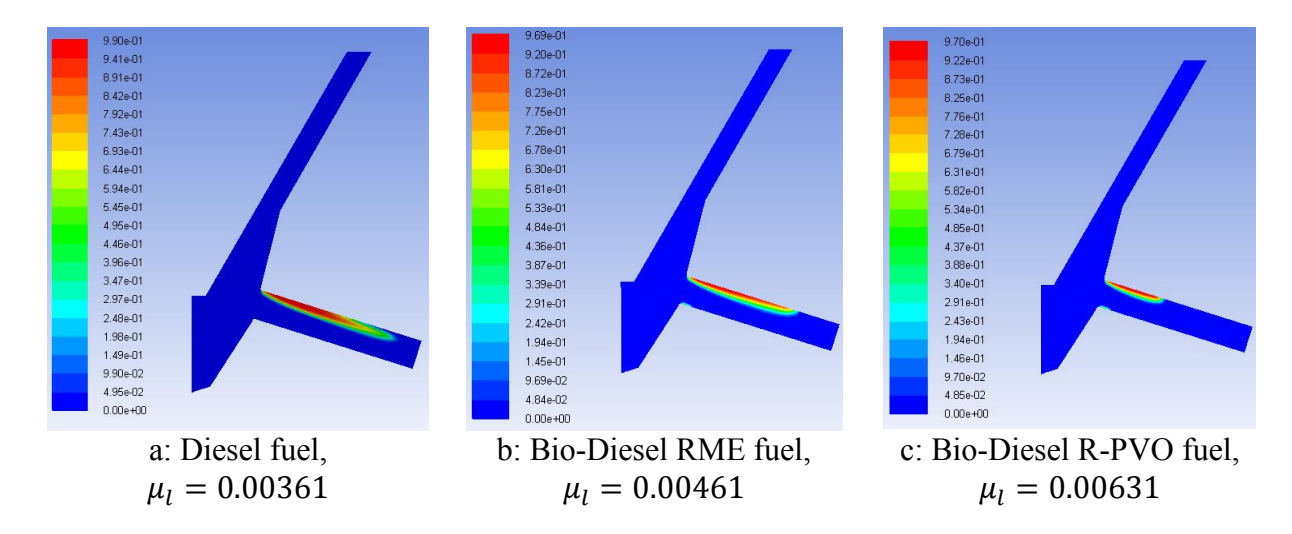


Figure 13. Distribution of vapor volume fraction in mid-plane of the nozzle for three different fuels when $p_{in} = 30MPa$ and $p_{back} = 3MPa$

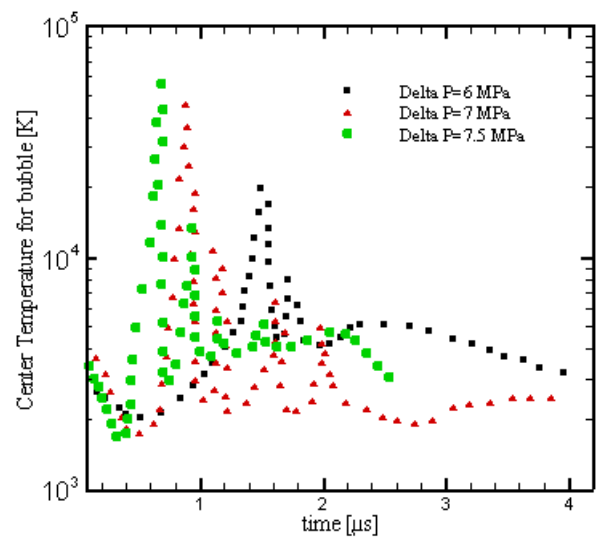
An Eulerian/Lagrangian code was introduced in our previous paper [15]. In the mentioned code, velocity and pressure were calculated and then used to track bubble inside Winklhofer *et al.* [5] rectangular shape nozzle. The results from the mentioned code were completely validated using two different experimental data.

Bubble Center Temperature During Implosion In this section, bubble temperature inside Winklhofer rectangular shape nozzle will be investigated [5]. The vapor inside a collapsing (imploding) bubble was treated as a calorically perfect gas despite the fact that the resulting temperature inside the bubble clearly involves real gas effects of dissociation and ionization.

Finite volume method was used to calculate pressure and velocity at each time step using Eulerian scheme. Inside finite volume method, SIMPLE algorithm was used for pressure and velocity linkage. Random number generation was also used to calculate turbulent velocity in x and y direction. Finally, after obtaining Eulerian solution, Lagrangian solution was utilized by utilizing one-way coupling. Modified Rayleigh-Plesset equation was used to calculate dynamic behavior of a vapor bubble. Forces applied to bubble were used in Newton's second law to calculate bubble's position after each time step. The time steps used in these calculations were on the order of 10^{-19} s, since bubble collapse occurs very rapidly. Finally, to decrease calculation cost, adaptive time steps were used.

Figure 14 shows center temperature of bubble versus elapsed time while bubble is moving inside Winklhofer nozzle. According to Fig. 14, increasing pressure difference can increase bubble center temperature up to 56269 K when pressure difference is 7.5 MPa. When pressure difference is 6 MPa, bubble center temperature is noticeably lower. Furthermore, as pressure difference increases, time interval for changing bubble center temperature decreases dramatically. In other words, as Fig. 14 shows, when pressure difference is 6 MPa, time interval is nearly 4 μ s, while increasing pressure difference up to 7 MPa, can reduce time interval to 3.8 μ s. Interestingly, when pressure difference reaches to 7.5 MPa, time interval reaches to 2.6 μ s, which shows a highly nonlinear behavior in the bubble center temperature.

Figure 15 shows bubble center temperature versus initial bubble radius for three different pressure differences. According to Fig. 15, when pressure difference is 6 MPa, increasing initial bubble radius can slightly change bubble center temperature. As pressure difference increases to 7.5 MPa, effect of initial bubble radius on bubble center temperature will also increase.



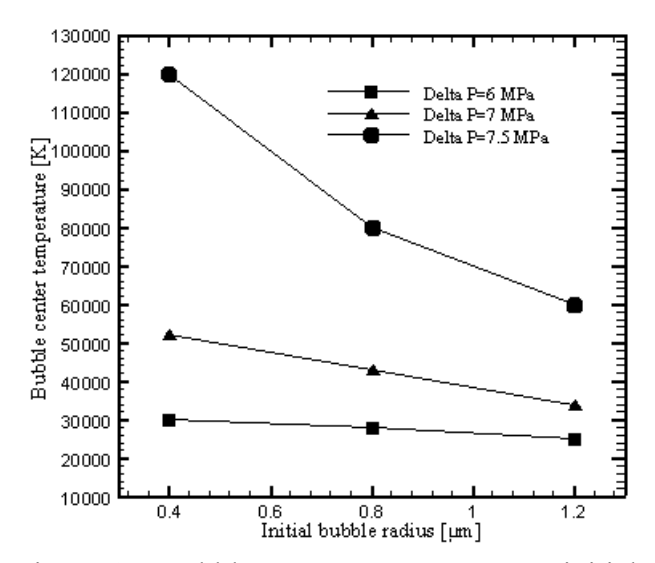


Figure 14. Bubble center temperature *vs.* elapsed time as a function of pressure difference.

Figure 15. Bubble center temperature *vs.* initial bubble radius as a function of pressure difference.

CONCLUSIONS

Flow inside a real size Diesel injector nozzle was modeled under different boundary conditions. Validation was also performed by comparing current numerical results with experimental results obtained by Winklhofer *et al*. The cavitation model was verified and afterward $k - \varepsilon$ turbulence model was chosen since it had better agreement with experimental results in comparison with $k - \omega$ turbulence model. Due to symmetric structure of the real size six-hole Diesel injector nozzle and for decreasing computational time only one-sixth of it was modeled. The results obtained in this study are as follow:

- 1- Mass flow rate in different pressures by increasing needle lift increases at first but then remains nearly constant.
- 2- Discharge coefficient by increasing cavitation number in different needle lifts increases. In high needle lift discharge coefficient remains stable after a definite cavitation number. In low needle lifts, discharge coefficient has consistently upward trend.
- 3- By decreasing outlet pressure in the cases that the carrying liquid is Diesel fuel, length of cavitation increases and when outlet pressure is 1 *MPa* cavitation reaches to the orifice outlet.
- 4- Length of cavitation region by increasing needle lift increases. In low needle lift, surprisingly cavitation occurs outside of the nozzle's orifice.
- 5- In different fuel types, mass flow rate by increasing pressure difference increases at first but then remains stable. Due to lower density of Diesel fuel in comparison with bio-Diesel fuel, mass flow rate of Diesel fuel is lower. Moreover, for two types of bio-Diesel, the one that has greater surface tension experiences higher mass flow rate.
- 6- In three types of fuel, discharge coefficient by increasing cavitation number increases at first but then remains stable.
- 7- In different fuels with similar boundary conditions, those fuels that have lower surface tension experience longer cavitation area in the nozzle's orifice.
- 8- The peak for bubble center temperature increases as pressure difference increases in the Winklhofer *et al.* [5] nozzle.
- 9- Increasing bubble initial radius can decrease the imploding bubble center temperature. In higher pressure difference nozzles, increasing bubble initial radius can decrease center pressure of bubble more severely.

ACKNOWLEDGEMENTS

This research was supported by the Naval Surface Warfare Center, Panama City Division, Florida under the supervision of Dr. Frank J. Crosby and facilitated by Dr. Quyen Huynh via TriCircle Company. It was also supported by the National Science Foundation by the research grant NSF CBET-1642253 monitored by Dr. Jose Lage. The third author gratefully acknowledges the financial support from Florida International University in the form of an FIU Presidential Fellowship. The views and conclusions contained herein are those of the authors and should not be interpreted as necessarily representing the official policies or endorsements, either expressed or implied, of NAVY or NSF, or the U.S. Government.

REFERENCES

- [1] Roth, H., Gavaises, H. and Arcoumanis, C. [2002], Cavitation Initiation, its Development and Link With Flow Turbulence in Diesel Injector Nozzles. *Society of Automotive Engineers International (SAE)* paper 2002-01-0214.
- [2] He, L. and Ruiz, F. [1995], Effect of Cavitation on Flow and Turbulence in Plain Orifice for High Speed Atomization. *Atomization and Sprays*, Vol. 5, No. 6, pp 569-584.
- [3] Bergwerk, W. [1959], Flow Pattern in Diesel Nozzle Spray Holes, *Proceedings of the Institution of Mechanical Engineers*. Vol. 173, pp 655-660.
- [4] Bode, J., Chaves, H., Obermeier, F. and Schneider, T. [1991], Influence of Cavitation in Turbulent Nozzle Flow on Atomization and Spray Formation of a Liquid Jet, *Proc. Sprays and Aerosols*, ILASS Europe.
- [5] Winklhofer, E., Kull, E., Kelz, E. and Morozov. A. [2001], Comprehensive Hydraulic and Flow Field Documentation in Model Throttle Experiments Under Cavitation Conditions. *Proceedings of the ILASS-Europe Conference*, Zurich, Schwitzerland, pp 574–580.
- [6] Schmidt, D. and Corradini, M. [2001], The Internal Flow of Diesel Fuel Injector Nozzles: A Review, *Int. J. Engine Res.*, Vol. 2, No. 1, pp 1–22.
- [7] Brennen, C. E. [1995], Cavitation and Bubble Dynamics, Oxford University Press, Oxford, UK.
- [8] Jospeh, D. D. [1998], Cavitation and the State of Stress in a Flowing Liquid, *J. Fluid Mech.*, Vol. 366, pp 367–378.
- [9] Giannadakis, E., Gavaises, M. and Arcoumanis, C. [2008], Modelling of Cavitation in Diesel Injector Nozzles, *J. Fluid Mech.*, Vol. 616, pp 153–193.
- [10] <u>Saha</u>, K. and <u>Li</u>, X. [2015], Assessment of Cavitation Models for Flows in Diesel Injectors With Single- and Two-Fluid Approaches, *J. of Engineering for Gas Turbines and Power*, Vol. 138, No. 1, pp 011504; doi: 10.1115/1.4031224.
- [11] Schnerr, G. H., Sauer J. and Yuan W. [2001], Modeling and Computation of Unsteady Cavitation Flows in Injection Nozzles, *Mécanique & Industries*. Vol. 2, pp 383-394.
- [12] Singhal, A. K., Athavale, M. M., Li, H. and Jiang, Y. [2002], Mathematical Basis and Validation of the Full Cavitation Model, *ASME Journal of Fluids Engineering*. Vol. 124, pp 617-625.
- [13] Zeidi, S. M. J. and Mahdi, M. [2015], Investigation Effects of Injection Pressure and Compressibility and Nozzle Entry in Diesel Injector Nozzle's Flow, *J. Appl. Comp. Mech., Vol.* 2, pp 83–94.
- [14] Zeidi, S. M. J. and Mahdi, M. [2015], Effects of Nozzle Geometry and Fuel Characteristics on Cavitation Phenomena in Injection Nozzles, The 22st Annual International Conference on Mechanical Engineering-ISME 2014, available online at http://www.civilica.com/EnPaper-ISME22 394.html.
- [15] Zeidi, S. M. J. and Mahdi, M. [2015], Investigation of Viscosity Effect on Velocity Profile and Cavitation Formation in Diesel Injector Nozzle, 8th International Conference on Internal Combustion Engines 2014, ISBN 978-600-91530, available online at http://www.civilica.com/EnPaper-ICICE08_055.html.

- [16] Lee, W. G. and Reitz, R. D. [2010], A Numerical Investigation of Transient Flow and Cavitation Within Minisac and Valve-Covered Orifice Diesel Injector Nozzles, *J. of Engineering for Gas Turbines and Power*. Vol. 132, No. 5, pp 052802-052810.
- [17] Salvador, F. J., Romero, J. V. and Rosello, M. D. [2010], Validation of a Code for Modeling Cavitation Phenomena in Diesel Injector Nozzles, *J. of Math. Comput. Model.* Vol. 52, pp 1123–32. [18] Som, S., Ramirez, A. I. and Longman, D. E. [2011], Effect of Nozzle Orifice Geometry on Spray, Combustion, and Emission Characteristics Under Diesel Engine Conditions, *Fuel*, Vol. 90, pp 1267–76.
- [19] Jia, M., Xie, M. and Liu, H. [2011], Numerical Simulation of Cavitation in the Conical Spray Nozzle for Diesel Premixed Charge Compression Ignition Engines, *Fuel*, Vol. 90, pp 2652–61.
- [20] He, Z., Zhong, Z., Wang, Q., Jiang, Z. and Fu, Y. [2013], An Investigation of Transient Nature of the Cavitating Flow in Injector Nozzles, *Applied Thermal Engineering*, Vol. 54, pp 56-64.
- [21] Sun, Z., Li, G., Chen, C., Yu, Y., Gao, G. [2015], Numerical Investigation on Effects of Nozzle's Geometric Parameters on the Flow and the Cavitation Characteristics Within Injector's Nozzle for a High-Pressure Common-Rail DI Diesel Engine, *Energy Conversion and Management*, Vol. 89, pp 843-861.
- [22] Zeidi, S. M. J. and Mahdi, M. [2015], Evaluation of the Physical Forces Exerted on a Spherical Bubble Inside the Nozzle in a Cavitating Flow With an Eulerian/Lagrangian Approach, *European J. of Physics*, Vol. 136. No. 6, pp 065041; doi:10.1088/0143-0807/36/6/065041.
- [23] Mulemane, A., Han, J. S., Lu, P. H. and Yoon, S. [2004], Modeling Dynamic Behavior of Diesel Fuel Injection Systems. *SAE Technical Paper* No. 2004-01-0536.
- [24] Som, S. [2009], Development and Validation of Spray Models for Investigating Diesel Engine Combustion and Emissions. *Ph.D. Dissertation*, University of Illinois at Chicago, USA.
- [25] Salvador, F. J., Martinez-Lopez, J., Caballer, M. and De Alfonso, C. [2013], Study of the Influence of the Needle Lift on the Internal Flow and Cavitation Phenomenon in Diesel Injector Nozzles by CFD Using RANS Methods. *Energy Conversion and Management*, Vol. 66, pp 246–56.
- [26] Payri, R., Salvador, F. J., Gimeno, J. and De la Morena, J. [2009], Study of Cavitation Phenomena Based on a Technique for Visualizing Bubbles in a Liquid Pressurized Chamber. *Int. J. Heat Fluid Flow*, Vol. 30, pp 768–77.
- [27] Martinov, S. [2005], Numerical simulation of Cavitation Process in Diesel Fuel Injectors. *Ph.D. Dissertation*. The University of Brighton, UK.